Revealing the Molecular Identity of Defect Sites on PbS Quantum Dot Surfaces with Redox-Active Chemical Probes

Carolyn L. Hartley and Jillian L. Dempsey*

Department of Chemistry, University of North Carolina, Chapel Hill, North Carolina 27599 – 3290

Abstract: Defects arising on the surfaces of semiconductor quantum dots (QDs) limit the applications of these otherwise promising materials. Efforts to rationally passivate these sites using chemical methods, however, are limited by a lack of molecular-level understanding of surface defects. Herein we report the application of redox-active chemical probes ($E^{\circ\prime}$ = −0.48 - −1.9 V vs. $Fc^{+/0}$) coupled with spectroscopic tools (NMR, XPS, and UV-Vis-NIR) to gain insight into the molecular-level nature and reactivity of defects at PbS QD surfaces. First, Pb ion-based traps coordinated by oleate ligands are studied by reaction with outer-sphere reductants, wherein reduction of a subpopulation of Pb^{2+} ions promotes ligand displacement. We observe a correlation between this reactivity and QD size wherein minimal ligand displacement occurs in small QDs (2.6 nm) but up to ca. 15% of ligands are displaced with larger QDs (> 4 nm). The strength of the reductant also has a significant impact; with QD size held constant, more potent reductants induce a higher extent of ligand displacement than mild reductants. Finally, chalcogenide-based defects (disulfides) are interrogated with selective trialkylphosphine reagents. Comparison of QD reactivity with phosphine probes reveal that large PbS QDs possess a greater proportion of native disulfide defects than small QDs. Collectively, this work yields insight into the identities, likely structural environments and reduction potentials of targeted defect sites, thus providing a detailed picture—and roadmap for passivation—of common QD surface defects.

1. Introduction

Colloidal semiconductor quantum dots (QDs) are a promising class of materials with potential applications in photovoltaics,[1,2] commercial displays,[3] and photoredox catalysis systems,[4,5] to name a few. However, commercialization of many QD-based optoelectronic devices has seen only limited success; this is largely due to the low charge transport efficiencies observed relative to bulk semiconductor materials. The cause for these low efficiencies can in part be attributed to performance-limiting defects at QD surfaces, such as underpassivated metal or chalcogenide ions, and can result in mid-gap electronic trap states.[6,7] Such states can trap excited electrons or holes, leading to low photochemical quantum yields and hindered charge transfer between nanocrystals within a device. Surface defects are present on as-synthesized QDs, and their occurrence and routes for passivation have consequently been a major area of study.[6–11] For instance, techniques such as emission spectroscopy and electrochemistry have traditionally been used to establish the presence and approximate energies of mid-gap trap states.[12–18] Though useful, such methods are limited by the insight they may provide regarding the *molecular identity* and *reactivity* of specific defects at the QD surface. [19]

Indeed, QD surface defects are often ill-defined, making targeted passivation approaches challenging. One tactic to elucidate the molecular-level details of QD surfaces—with the aim of controlling these defects sites—is the use of chemical probes. Chemical probes are molecular reagents that react predictably with specific sites at the QD surface, and the resulting reactivity in turn can reveal details about the native QD surface structure.[20–25] Chemical probes may be classified as either ligand-based probes, or redox-active probes depending on the type of reactivity they engage in at the QD surface (**Scheme 1**).[19]

Scheme 1. Approaches to studying surfaces defects through reaction of QDs with (i) ligand-based (shown here for metal ion defects) or (ii) redox-active chemical probes

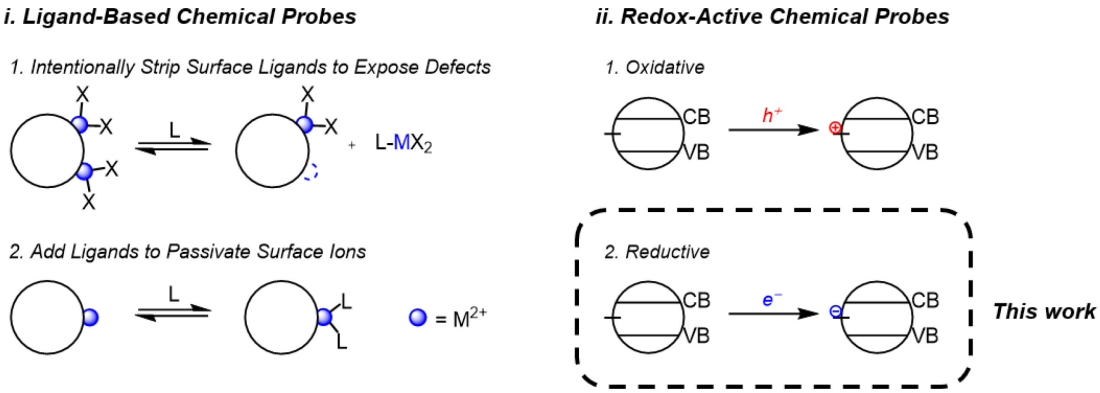

Similarly, redox reactivity has been key to elucidating metal-based surface defects. A recent study by our group revealed that addition of $Na[C_{10}H_8]$ ($E^{o\prime}$ = −3.1 V vs. $Fc^{+/0}$) to CdSe QDs led to reduction of surface Cd^{2+} ions with concomitant displacement of charge-balancing anionic ligands, yielding putative Cd^0 sites on the QD surfaces.[23] This example illustrates the redox reactivity of surface Cd^{2+} sites and the displacement of anionic ligands via an electron-promoted X-type ligand displacement mechanism in response to surface metal ion charging. The reduction of Cd^{2+} surface sites was also recently reported by Pu et al. upon applying an electrochemical bias to CdSe QD thin films passivated with cadmium carboxylate ligands.[27] DFT studies by Voznyy et al. and du Fossé et al. have explored the impact of charging at the surfaces of semiconductor QDs and predicted that the dimerization of surface metal ions induced by charging serves as a source of mid-gap trap states.[28,29] Collectively, these examples highlight how redox-active chemical probes may be employed to better understand QD surface structure, as well as inform on accessible redox-active surface moieties.

While the combined efforts of the aforementioned studies have yielded insight into QD surface structure, there remains a need for a systematic investigation of the molecular nature (atomic identity, bonding environment, oxidation state, or reduction potential) and reactivity of these surface defects . Indeed, many of the examples noted above focused on identifying the structure or oxidation state of likely defect sites but stopped short of exploring their redox reactivity—an important indicator of the specific environment of a given defect—in tandem. Additionally, QD size is known to impact which bonding environments—and therefore which possible defects—may exist at the surface, yet this variable has been underexplored to date.[22,30,31] Importantly, the redox properties of defect sites are expected to have significant influence on the QD reactivity in multi-component systems, as well as have major implications in QD charging or remote chemical doping processes.

To this end, we herein report systematic investigations of defect sites on PbS QD surfaces using a series of redox-active chemical probes. PbS was selected as it is a widely studied and well understood QD material, and thereby serves as a relevant platform for redox-active defect sites. We first establish the reactivity between a moderately reducing organometallic reductant, cobaltocene, with metal-based surface sites on 4.1 nm PbS QDs and then study the impact of varying QD size and potency of the reductant. Finally, we explore other redox-active defect sites at the surface by employing selective trialkylphosphine reagents to selectively probe chalcogenide defects. Our studies reveal the presence

of both metal and chalcogenide defect structures at PbS QD surfaces. By studying the reactivity of these defect sites with redox-active chemical probes, we elucidate their molecular-level nature and reduction potentials. In doing so, we deepen understanding of QD surface defects and routes to intentionally passivate or induce them.

2. Experimental Methods

General Considerations. All syntheses were performed under a nitrogen environment using standard Schlenk techniques. All experiments were performed or set up in a dry nitrogen-filled glovebox (MBraun) unless otherwise noted. Solvents used in the glovebox (toluene, tetrahydrofuran, acetonitrile) were purified over an alumina column and dispensed from a dry argon-atmosphere solvent system (Pure Process Technologies) and then dried over activated 3 Å molecular sieves. NMR solvents were similarly stored over activated 3 Å molecular sieves, and in the case of THF-d_8 further dried over an alumina plug.

Chemicals. Lead(II) oxide (PbO) (99.999% trace metals basis), oleic acid (OA) (90%), 1-octadecene (ODE) (90%), hexamethyldisilathiane ($(TMS)_2S$) (synthesis grade), tri-*n*-butylphosphine (Bu_3P) (mixture of isomers, 97%), 1,3,5-trimethoxybenzene (TMB) (Reagent Plus ≥99%) and 7,7,8,8-tetracyanoquinodimethane (TCNQ) were purchased from Sigma-Aldrich and used as received. Sodium hydroxide was purchased from Fisher Scientific and used as received. Cobaltocene ($CoCp_2$) (≥98%) was purchased from VWR and purified by dissolving in toluene in a glovebox in the dark, filtering off insoluble particulates, and removing solvent under vacuum, followed by sublimation of the solid in the dark prior to use. Purified cobaltocene was stored in a −30 ºC freezer under inert atmosphere. Decamethylcobaltocene ($CoCp^*_2$) was purchased from Sigma-Aldrich and recrystallized from cold pentane before use and then stored in a −30 ºC freezer in a glovebox. Toluene-d_8 and THF-d_8 were purchased from Cambridge Isotope Laboratories. All other solvents used were purchased from Fisher Scientific or VWR.

PbS Synthesis and Purification. PbS QDs were synthesized using a previously reported literature procedure.[22] QDs ranging in diameter from 2.6 to 4.9 nm were prepared by varying the molar ratio of OA to PbO used to prepare the $Pb(oleate)_2$ precursor as well as the injection temperature of the $(TMS)_2S$. In general, higher OA:PbO ratios and higher injection temperatures resulted in larger nanocrystals (**Table S1**). The QDs were purified rigorously by repeated precipitation and centrifugation cycles to isolate the nanocrystals from excess ligand, solvent and reaction byproducts. For QDs used in direct size comparison studies, purification procedures were the same across all batches. For these batches (2.6 nm, 3.8 nm, 4.1 nm, 4.9 nm, feature in Section 3.3), the crude reaction mixture was precipitated with acetone and divided among centrifuge tubes and centrifuged. The supernatant was decanted, and the QD solid was dispersed in 1 – 2 mL pentane or toluene and precipitated with 12 mL acetone, sonicated, and centrifuged. This step was repeated once. The resulting solid was dispersed in 1 mL pentane and precipitated with a 1:1 mixture of acetone and methanol, sonicated, and centrifuged. This step was repeated a total of three to four times. The QDs were dispersed in 1 mL pentane, precipitated with 12 mL methanol and centrifuged. The QDs were then dispersed in 1 mL pentane and precipitated with 9 mL of a 1:2 mixture of acetone:methanol, sonicated, and centrifuged. This step was repeated a total of two to three times. Finally, the QDs were dispersed in 1 mL pentane, precipitated with 12 mL acetone, and centrifuged a total of three times. For the largest batch of QDs (4.9 nm) prepared with a large excess of oleic acid, we found that filtering the QD solution over a glass fiber filter paper plug between purification steps further helped to get rid of excess $Pb(oleate)_2$. The purified solid was then dispersed in pentane, transferred to a 20 mL vial, and dried via evaporation.

For samples used in other studies, purification proceeded with minor variations to the procedure described above. The QDs were stored as a solid in an inert-atmosphere glovebox. QD size and extinction coefficients at 400 nm were determined using the sizing curve reported by Moreels et al.[32]

UV-Vis-NIR Absorbance Studies. UV-Vis-NIR absorbance data was collected on an Agilent Cary 60 or Cary 5000 spectrophotometer. Samples of QDs were prepared in toluene (1 – 5 μM) and ~3 mL of this solution were added to a custom-made quartz cuvette with an adapted 14/20 ground-glass joint. The cuvette was equipped with a micro stir bar and then capped with a rubber septum that was secured with electrical tape and copper wire. A solution of cobaltocene was prepared in toluene (15 mM) and then loaded into a gas-tight locking Hamilton syringe. The charged needle was locked and the end stuck into a separate rubber septum to avoid exposure to air. The cuvette and syringe were then brought out of the glovebox and the cobaltocene was added

incrementally by syringe, stirring for approximately 30 seconds after each addition to ensure thorough mixing before collecting a spectrum. Samples for long timescale studies were prepared in cuvettes sealed with Kontes valves and shielded from light.

NMR Studies. ^{1}H NMR spectra were collected on a 600 MHz Bruker NMR spectrometer with a cryoprobe. Unless noted otherwise, titration studies were prepared by adding 600 μL of a 30 μM QD stock solution in toluene-d_8 to J-Young NMR tubes. An internal standard stock solution was then prepared by dissolving ~15 mg of 1,3,5-trimethoxybenzene in 1.5 mL toluene-d_8, and then 50 μL was added to each NMR tube. A 50 mM solution of redox reagent was prepared in toluene-d_8 and added in increments of 0, 50, 100, 500, and 1000 equivalents per QD to the NMR tubes at staggered times to ensure that all samples mixed for the same amount of time (3 hours) before collecting NMR spectra. Spectra were collected with 12 scans and a d1 delay time of 30 seconds. The absolute number of bound and free ligands per QD were determined by spectral fitting with MestReNova software (**Figure S1**). ^{31}P{^{1}H} NMR spectra were collected on a 500 or 600 MHz Bruker NMR spectrometer.

XPS Sample Preparation. Samples for X-ray photoelectron spectroscopy (XPS) analysis were measured on gold-coated silicon wafers that had been sonicated for 2 minutes in 190 proof ethanol and dried in air prior to use to remove residual carbon species. Solutions of QDs in toluene (typically ~10 μM) reacted with 0, 50, 100, 500 or 1000 equiv. cobaltocene for 21 hours and then the QDs isolated by precipitation with acetonitrile. The isolated nanocrystals were redispersed in toluene and were drop cast onto the wafers until a brown film was visible by eye. The XPS samples were loaded onto a sample holder in a nitrogen-filled glovebox and transported to the XPS facility in a sealed glass tube, which was then loaded onto the instrument in an inert-environment glovebag.

TEM Sample Preparation. Samples for Transmission electron microscopy (TEM) imaging were prepared by drop casting dilute solutions of QDs in pentane that were filtered through 2 μm PTFE syringe filters onto TEM grids (Ultrathin carbon film on lacey carbon support film, 400 mesh, copper) under ambient conditions. The grids dried in air and were then conditioned overnight under vacuum to remove any trace volatiles. Images were collected on a Thermo Scientific Talos F200X S/TEM at an accelerating voltage of 200 kV and with a 70 μm objective aperture.

3. Results and Discussion

3.1. A System for Studying Redox-Active Defect Sites on PbS Surfaces

Oleate-capped PbS QDs ranging in size from 2.6 to ca. 5 nm in diameter provide a versatile platform for interrogating redox-active defects on QD surfaces. The size range explored here provides a means to access QDs with a range of band edge potentials as well as different morphologies, surface facets and stoichiometries which are known to vary as a function of QD size for PbS.[22,30,31,33] Varying QD size in our studies thereby provides additional insight into the molecular nature of reactive surface species.

Redox-active chemical probes were selected to span potency from strong ($E^{o\prime}$ = −1.9 V vs. $Fc^{+/0}$) to weak ($E^{o\prime}$ = −0.48 V vs. $Fc^{+/0}$) (**Table 1**). As other works have investigated oxidation of PbS QD surfaces,[26] we focus here on the impact of reductive chemical probes. With this wide array of reductants, we demonstrate that it is possible to vary the driving force of surface reduction and, in effect, target specific sites to rationally passivate undesired surface defects.

3.2. PbS QDs Display Surface Reactivity with $CoCp_2$

The reactivity between a mid-size batch of PbS QDs (4.1 nm diameter) was first established with the moderate reductant cobaltocene ($CoCp_2$, $E^{o\prime}$ = −1.3 V vs. $Fc^{+/0}$). $CoCp_2$ has been previously shown to undergo ground state charge transfer with PbS QDs and does not display any deleterious side chemistry.[34,35]

Upon reduction of a colloidal QD by $CoCp_2$, the donated electron can either occupy a delocalized conduction band electronic state or be confined to localized electronic states at the surface (**Figure 1a**). In order to assess whether $CoCp_2$ is able to reduce the 4.1 nm PbS QD conduction band (CB) edge state, the electron transfer reaction was monitored using UV-Vis-NIR absorbance spectroscopy. Absorbance spectroscopy is commonly employed to gauge band edge charging with excess electrons or holes; upon reduction of the CB or oxidation of the valence band (VB), a bleach of the excitonic absorbance feature will be observed due to the lowered probability of exciting a carrier into an already-filled state.[35,36] The absorption spectra of the 4.1 nm QDs in toluene

before and after addition of 500 equiv. $CoCp_2$ (per mol QD) are shown in **Figure 1b**. No excitonic bleach (λ_{max} = 1186 nm) is observed, indicating that band edge reduction by $CoCp_2$ is energetically unfavorable even with a large excess of reductant. While previous studies observed interfacial electron transfer from $CoCp_2$ into CB states of similarly sized oleate-capped PbS QDs (≥ ~ 4.2 nm in diameter),[35] our observations likely differ from this prior report as this previous work was performed on QD thin films rather than in solution.

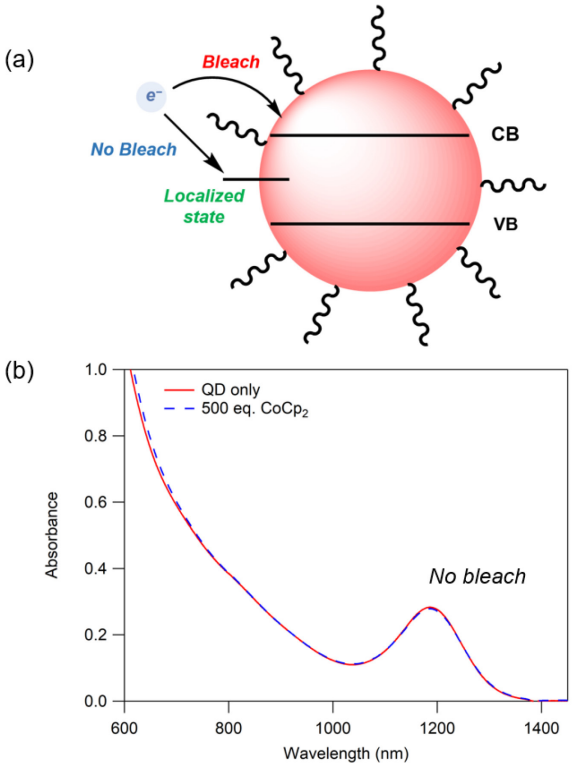

Figure 1. (a) Diagram depicting the optical response observed by absorbance spectroscopy upon reduction of either the band edge state or a localized surface state. (b) UV-Vis-NIR absorption spectrum of 4.1 nm QDs (2.5 μM) in toluene before (red) and after (blue) addition of 500 equiv. $CoCp_2$.

Although no band edge reduction was observed by UV-Vis-NIR absorbance spectroscopy, we anticipated that $CoCp_2$ was a sufficiently strong reductant to reduce localized surface states, as has been postulated previously.[35] In order to interrogate reduction of the surface directly, titration studies were performed using ^{1}H NMR spectroscopy. NMR spectroscopy is a convenient method to probe QD surface chemistry as it allows for quantification of the capping oleate ligands bound to surface Pb ions. The alkene proton resonance of the oleate ligands may be used to differentiate between bound vs. free ligands in solution. The bound oleate ligand resonance is broad and appears at 5.66 ppm, whereas the free oleate resonance are sharper and shifted up-field (5.48 ppm).[22,37–39] Characterization of as-synthesized 4.1 nm QDs reveal an average bound ligand coverage of 173 ± 5 oleates per QD.

Addition of excess $CoCp_2$ (0 – 1000 equiv.) to the PbS QDs in toluene-d_8 results in dissociation of a portion of bound oleate ligands that increases with equivalents of reductant added (**Figure 2**). The 4.1 nm QDs lose an average of 14.7 ± 3.2% of initially bound oleate ligands with addition of up to 1000 equiv. $CoCp_2$; this corresponds to approximately 25 oleate ligands displaced per QD. Importantly, the total number of ligands (bound + free) remains constant throughout the course of the titration, indicating that the QDs remain stable in solution even in the presence of large excesses of reductant (**Figure S1 – S2**). X-ray photoelectron spectroscopy (XPS) studies confirm that isolated PbS QDs reacted with an excess of $CoCp_2$ do not have any significant changes in their Pb:S ratio (**Table S2**). The observed ligand loss without a corresponding loss of surface Pb atoms therefore suggests that the detected free ligand is due to liberation of X-type anionic oleates, and not Z-type $Pb(oleate)_2$ fragments, upon reduction. This observation is consistent with the electron-promoted X-type ligand displacement phenomenon previously reported for CdSe QDs,[23] and these data thereby provide direct evidence that surface Pb^{2+} ions are reduced by $CoCp_2$.

Within our system we propose that oleate-bound Pb^{2+} surface ions are reduced to Pb^0 concurrent with ejection of bound anionic oleate ligands; reduction to form surface Pb^0 sites is expected to be stable and would be consistent with reports of Cd^0 formation upon reduction of Cd^{2+} ions at the surfaces of CdSe nanocrystals.[23,40–43] Though formally plausible, Pb^{1+} ions are anticipated to be unstable and, if formed, would likely dimerize with neighboring Pb ions as has been postulated in recent computational studies.[28,29] We were unable to detect direct evidence for Pb-Pb dimers or formation of Pb^0 atoms using XPS spectroscopy (**Figure S3**); however, this could be due to the limited sensitivity of XPS to minor surface subpopulations on QDs. Therefore, the formation of these surface structures upon reduction of Pb^{2+} ions

and displacement of oleate ligands cannot be ruled out.

In addition to monitoring resonances corresponding to the surface capping ligands in the ^{1}H NMR spectra, the reductant $CoCp_2$, and its oxidized product $[CoCp_2]^+$, are also readily detected in the ^{1}H NMR spectra. At all equivalents added (50 – 1000 equiv.), the NMR resonance for paramagnetic $CoCp_2$ is observed at −52 ppm (**Figure S4**). The presence of $CoCp_2$ in the QD samples indicates that while a portion of the reducing agent reacts with the QD (as evidenced by liberation of X-type oleate ligands), not all of the $CoCp_2$ added reacts on the hours-long timescale. Furthermore, a new broad feature is observed at 6.2 ppm after $CoCp_2$ is added (**Figure S1**). We tentatively assign this to the NMR resonance of the cyclopentadienyl protons of the oxidized cobaltocenium ion ($[CoCp_2]^+$). In support of this assignment, we isolated the putative $[CoCp_2]$[oleate] from a mixture of PbS QDs with excess $CoCp_2$ (see **SI**). $[CoCp_2]^+$ is expected to act as a counterion to both reduced surface sites as well as to liberated oleates as a cobaltocenium oleate salt, $[CoCp_2]$[oleate] (**Figure S5 – S10**).[44]

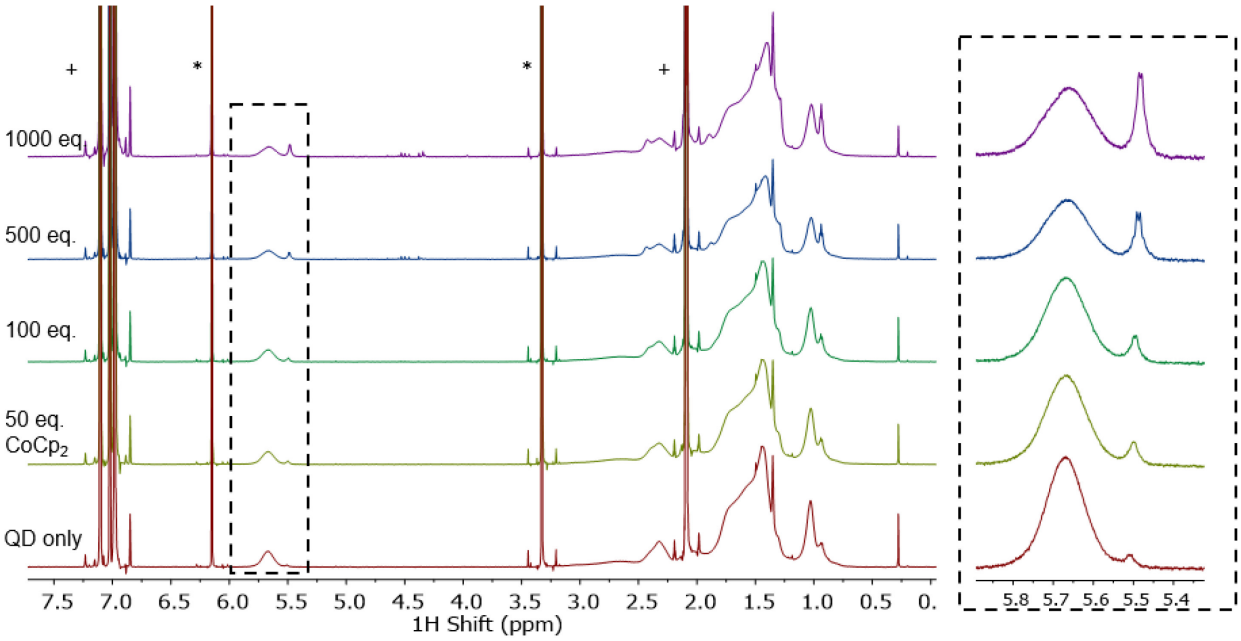

When samples are allowed to react over the course of days, the relative integration of the paramagnetic $CoCp_2$ resonance decreases (**Figure S11**). Concurrently, oleate ligands continue to dissociate from the QD surface (**Figure S11**). The slow and continued reactivity over hours and days point towards a gradual equilibration between $CoCp_2$ and surface Pb^{2+} ions. Therefore, all NMR titrations were carefully timed to ensure that all samples mixed for exactly the same period of time (3 hours) prior to collecting spectra to enable precise comparisons in the extent of surface reduction and oleate loss.

Additionally, it is important to note that ^{1}H NMR-silent redox processes are expected to occur in tandem with oleate displacement. For example, underpassivated Pb^{2+} sites or hydroxide-ligated Pb^{2+} ions have been postulated as PbS surface defects in the literature, though these would not be observable by our NMR experiments.[28,29,45] Attempts to detect the presence and reduction of these postulated Pb^{2+} surface sites by XPS (**Figure S12**) and FTIR (**Figure S13**) spectroscopies were inconclusive; however, we cannot eliminate the possibility of small subpopulations of these and similar metal-based sites on the surface reacting with added excess reductant.

3.3. QD Surface Reactivity Has A Marked Size Dependence

Having established measurable reactivity (i.e., surface Pb^{2+} ion reduction and oleate displacement) at the surfaces 4.1 nm PbS QDs upon addition of excess $CoCp_2$, we next sought to understand the dependence of surface redox reactivity on QD size. For PbS, QD diameter is known to influence the band edge potentials as well as the morphology and surface facets exposed.[22,30,31] To investigate the influence of these parameters, we prepared several batches of QDs that varied in diameter. Each batch was handled and purified similarly for relevant comparison. To that end, we found that samples prepared by another method[46] did not precisely follow the trends observed below, and we thus restrict our discussion to these samples prepared by the method reported by Hines and Scholes.[47] Three additional sizes of QDs—2.6, 3.8, and 4.9 nm—were prepared and characterized by UV-Vis-NIR absorbance spectroscopy, ^{1}H NMR spectroscopy, TEM, and XPS methods (**Table S3**, **Figures S14 – S17**). QDs larger than 5 nm are not compared herein due to problems with solubility and stability of those sizes prepared by the method of Hines and Scholes.[47]

In order to first probe whether $CoCp_2$ is able to directly reduce the CB states of any of these QDs, each sample was titrated with aliquots of $CoCp_2$ and the absorbance monitored via UV-Vis-NIR absorbance spectroscopy (**Figure S18 – S22**). As the 4.1 nm QDs did not show any evidence of CB charging, it was not expected that the smaller QDs (2.6 and 3.8 nm) would show an excitonic bleach, as their conduction band edge states are higher in energy. Notably, no excitonic bleach was observed for any of these four samples, indicating that even for the larger 4.9 nm QDs, $CoCp_2$ is too weak of a reductant to engage in ground state electron transfer to the CB edge states of PbS. Many of the PbS QD samples did display a minor red-shift (1 – 4 nm) of the excitonic absorbance feature. This red-shift is an established indicator of surface charging resulting from Coulombic repulsion with the delocalized exciton.[48]

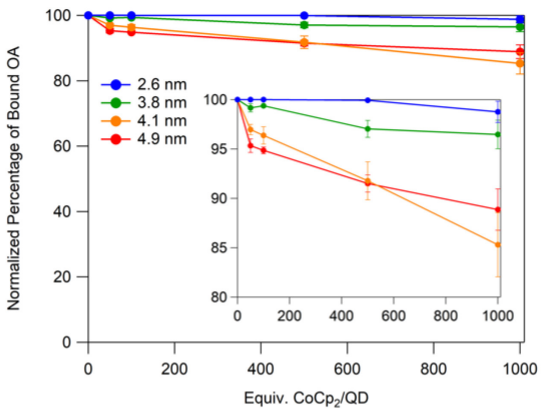

Figure 3. Comparison of different sizes of QDs with added $CoCp_2$, normalized for minor amounts of free ligand in QD only ^{1}H NMR spectra. Data points are the average of three repeated trials with standard deviation included as error bars. The lines between data points are a guide to the eye. Inset: Data plotted with smaller y-axis range for clearer depiction of trends.

Titrations of these three additional QD samples with $CoCp_2$ were then monitored with ^{1}H NMR spectroscopy in order to compare the extent of reactivity with added charge. Addition of excess of $CoCp_2$ (0 – 1000 equiv.) resulted in varying degrees of oleate displacement for the different sizes (**Figure S23 – S26**). The average percentages of bound oleate ligands (normalized for any minor amounts of free ligand present in the as-synthesized QD sample) are presented in **Figure 3**. The data show a clear trend of greater oleate loss with increasing QD size: after mixing for 3 hours with 1000 equiv. $CoCp_2$, 1.2 ± 1.1% of the bound oleates are displaced from 2.6 nm QDs, 3.5 ± 1.4% from 3.8 nm QDs, 14.7 ± 3.2% from 4.1 nm QDs, and 11.1 ± 2.1% from 4.9 nm QDs. The broad feature at 6.2 ppm attributed to $[CoCp_2]^+$ is observed in all QD samples with $CoCp_2$ added, as is the presence of paramagnetic $CoCp_2$ at −52 ppm.

We interpret the trend of greater amounts of displaced oleates observed for larger QDs by considering changes in the PbS QD surface environments with size. Several recent compelling works have demonstrated that PbS QDs transition from an octahedral morphology to a cuboctahedral shape with increasing diameter.[22,30,31] This in turn impacts the types of facets and bonding environments at the surface that are exposed. For example, small octahedral PbS QDs (< 3 nm) are known to be lead-rich with polar (111) facets exposed. Conversely, larger QDs tend to be more stoichiometric in Pb and S

ions, and it has been proposed that additional neutral (100) facets begin to appear on QDs larger than ~3 nm diameter.[22,30,31] Additionally, the larger QD sizes in this study possess lower ligand packing densities than the smaller QDs (**Table S3**) which suggests that the surfaces of larger QDs may be more accessible to reducing agents.

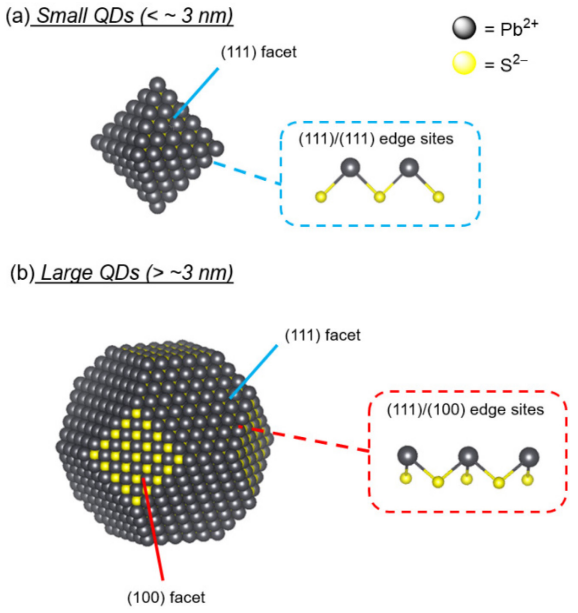

The size dependence of exposed Pb coordination environments at the surface likely impacts the extent of ligand displacement observed upon reduction by $CoCp_2$. Importantly, surface Pb^{2+} ions that are reduced by $CoCp_2$ to liberate oleate ligands are anticipated to be at approximately the same free energy (as quantified by their reduction potential) regardless of QD size. Therefore, the greater proportion of oleates displaced in larger QD sizes suggests that there is a larger relative number of those specific types of Pb^{2+} sites in larger QDs. While the NMR studies themselves cannot indicate distinct ligand bonding environments, the size dependence observed here suggest that the Pb^{2+} sites most likely to be reduced by $CoCp_2$ may be those at the edges between (111) and (100) facets as those appear on larger size QDs (**Figure 4**). Reduction of Pb^{2+} ions within the (100) facets present on the larger QDs is less likely due to the overall charge neutrality of those facets as well as being less sterically accessible than edge sites.[22,45].

3.4. The Extent of QD Surface Charging Tracks with Reductant Strength

In order to gain a more wholistic understanding of the redox reactivity of the surfaces of PbS QDs, we next probed the dependence of surface reactivity on the potency of the reductant employed. To do this, both milder and stronger reductants than $CoCp_2$ (**Table 1**) were reacted with PbS QDs and the extent of reactivity (i.e., oleate displacement in ^1H NMR studies) compared. For these redox-reagent dependence experiments, additional batches of PbS QDs ranging in size from ca. 3 – 5 nm were employed in addition to those studied in the size-dependence experiments above. These studies provide insight into the effect of driving force on surface reduction.

We first employed two reductants milder than $CoCp_2$, decamethylferrocene ($FeCp^*_2$) and Co(Cp)(dppe), and monitored their reactivity with 4.3 nm PbS QDs. Upon reaction of 4.3 nm QDs with ca. 500 equiv. of each redox agent, less ligand loss was observed compared with $CoCp_2$ as shown with ^1H NMR spectroscopy (**Figure S27**). Specifically, <1% oleate loss was observed upon addition of excess $FeCp^*_2$ and ~2.5 – 4% with added Co(Cp)dppe, compared with ~6% ligand displaced with added $CoCp_2$. This diminished reactivity with milder reducing agents illustrates the influence that the reductant strength has on the extent of surface charging.

Table 1. Chemical Redox Probes Used in This Work[34,49]

Chemical Probe	Reduction Potential ($E^{o\prime}$, V vs. $Fc^{+/0}$)	Energy vs. Vacuum[d] (eV)
Decamethylcobaltocene, $CoCp^*_2$	−1.91[a]	−3.22
Cobaltocene, $CoCp_2$	−1.33[b]	−3.80
Co(Cp)(dppe)[c]	−0.93[b]	−4.20
Decamethylferrocene, $FeCp^*_2$	−0.48[a]	−4.65

a. Reported conditions in CH_3CN with $[Bu_4N][PF_6]$

b. Reported conditions in CH_2Cl_2 with $[Bu_4N][PF_6]$

c. dppe = 1,2-bis(diphenylphosphino)ethane

d. Conversion to energy from reduction potential shown in SI

To further establish the relationship between surface charging and reductant strength, we next moved to a reductant stronger than $CoCp_2$, decamethylcobaltocene ($CoCp^*_2$). Due to the strongly reducing nature of $CoCp^*_2$ and estimated literature values for PbS CB edge potentials—ranging from −3 eV to ca. −4.2 eV (with respect to vacuum) across sizes from 2 nm to 8 nm, respectively—we anticipated that $CoCp^*_2$ could directly inject electrons into QD CB edge states.[33,35] Addition of 50 equiv. $CoCp^*_2$ to 4.9 nm PbS QDs in 1:1 THF: toluene resulted in a significant bleach of the excitonic absorption feature, as detected by UV-Vis-NIR absorbance spectroscopy, consistent with electron injection into the CB states (**Figure 5a**). Notably, the excitonic bleach recovers within minutes (**Figure S28**). This observation is consistent with a previous report by Koh et al. that suggested that delocalized CB electrons in PbS QDs may localize at surface sites over time.[35]

^{1}H NMR titrations were next performed to assess whether the more negative reduction potential of $CoCp^*_2$ has an impact on the amount of oleate displacement observed. Incremental addition of $CoCp^*_2$ (5 – 100 equiv.) to 4.9 nm QDs leads to a dramatic decrease in oleate coverage, with up to 60% of bound oleates lost (**Figure 5b**). Interestingly, the quantification of displaced oleate ligands corresponds closely with a 1:1 loss for each equivalent of $CoCp^*_2$ added up to 10 equiv., and then slightly greater ratio of approximately 1.2 – 1.4 oleates lost per equiv. $CoCp^*_2$ added with 25 – 100 equiv. (**Table S4**). The excess oleate ligands displaced per equivalent of $CoCp^*_2$ added suggests that there may be a more complex ligand displacement mechanism at play in the higher equivalent regime. For example, $CoCp^*_2$ may be capable of reducing spectroscopically silent surface states, the reduction of which could promote surface rearrangement leading to some Z-type ligand dissociation.

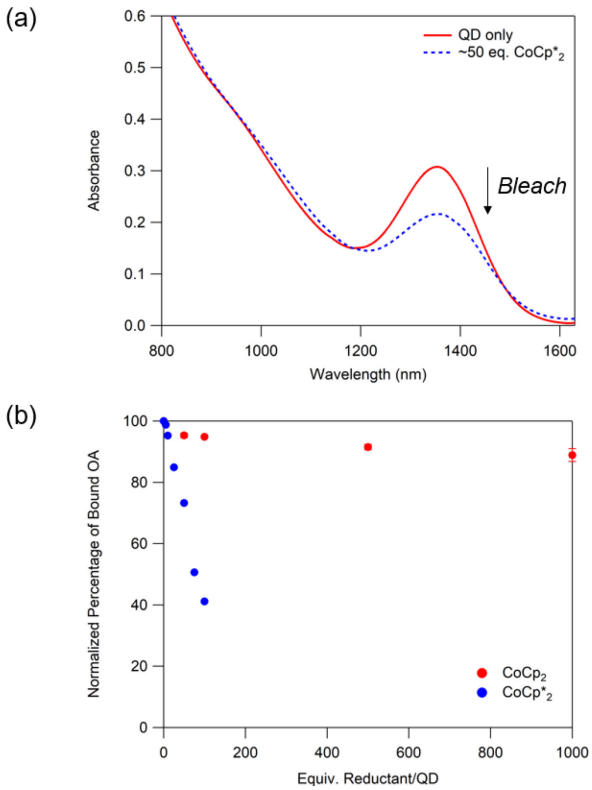

Figure 5. (a) UV-Vis-NIR absorption spectra of 4.9 nm QDs (2.5 μM) in 1:1 THF:toluene before (red) and after (blue) addition of ca. 50 equiv. $CoCp^*_2$. (b) Comparison of the percentage of bound oleate per QD in 4.9 nm PbS QDs (27.7 μM) with added $CoCp_2$ (red) and $CoCp^*_2$ (blue). NMR spectra of $CoCp^*_2$ titration in Figure S29.

Furthermore, unlike for milder reductants and $CoCp_2$, we observe complete consumption of the $CoCp^*_2$ as evidenced by lack of a paramagnetic resonance for $CoCp^*_2$ expected at ca. 45 ppm. Importantly, addition of $CoCp^*_2$ in greater excess (>100 equiv./QD) results in rapid QD precipitation, indicating that loss of a large percentage of passivating surface ligands leads to QD instability. The dramatic increase in oleate displacement observed with $CoCp^*_2$ addition is likely a direct result of the greater driving force for reduction of the same Pb surface sites that react with $CoCp_2$, as well as reduction of higher energy populations of Pb ions that are perhaps inaccessible to milder reductants even at high concentrations. Additionally, another pathway for surface reduction by $CoCp^*_2$ is also possible wherein electrons injected into the CB edge are subsequently trapped at lower energy surface sites as evidenced by the recovery of the excitonic bleach on a minutes-long timescale,[35] leading to further oleate ligand displacement upon localization at the surface. These surface reduction pathways may occur

simultaneously and are not necessarily mutually exclusive.

Overall, these studies reveal the marked impact of reductant strength on the extent of surface charging as indicated by the extent of oleate loss. The lesser degree of reactivity of the QD surface sites with reductants milder than $CoCp_2$, along with the more dramatic reactivity upon reaction with stronger reductants such as $CoCp^*_2$, suggests that the slow equilibration between $CoCp_2$ and PbS QD surface states observed arises because the reduction potential of $CoCp_2$ is approximately isoenergetic with the reduction potential of a portion of the surface Pb^{2+} sites (**Figure 6**). This equilibration leads to gradual oleate ligand displacement over time. These Pb^{2+} surface sites are not energetically accessible by the weaker reductants employed. By comparison, more potent reductants increase the driving force for surface Pb^{2+} ion reduction leading to more rapid and complete surface charging, as well as conduction band population.

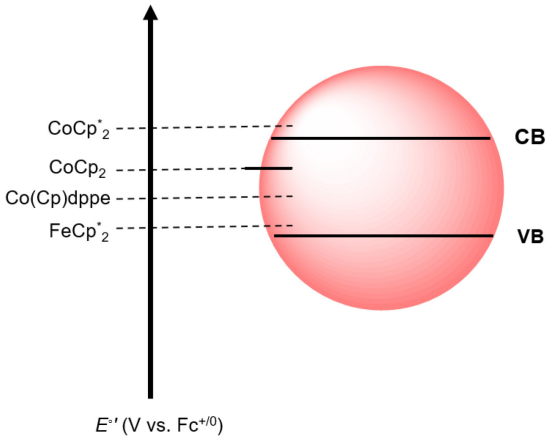

Figure 6. Depiction of the relative redox potentials of the redox-active probes used in this study versus band edge or surface-based electronic states in PbS QDs ranging in size from 2.6 to ca. 5 nm.

While the driving force for electron transfer from a reductant may in theory be predicted by comparing the reduction potential of the reagent with the reduction potentials of the localized surface and CB edge states of QDs, precise measurement of the latter values is quite challenging in practice. As such, our conclusions are not trivial. Though reduction potential values for band edge states have been reported for thin films of QDs using techniques such as photoelectron emission spectroscopy and electrochemistry, these values inherently differ from those describing colloidal QDs due to differences in the nanocrystal environment.[17,33,50] Additionally, the accuracy of reported values across all systems is questionable: variations in QD synthesis and purification methods, solvents and the influence of capping ligands via surface dipoles directly impact the absolute band edge positions.[51,52] As the reduction potentials of QD band edge and surface states are difficult to measure directly, the use of redox-active chemical probes spanning a wide range of reduction potentials therefore provides an indirect method to gauge the electronic state potentials based on the extent of reactivity observed by techniques such as UV-Vis-NIR absorbance or NMR spectroscopy.

3.5. Hypothesized Chalcogenide Defects may be Studied by Selective Probes

Following the above studies monitoring surface Pb^{2+} ion reduction by oleate ligand displacement, we sought to gain a more complete picture of other redox-active sites at PbS QD surfaces. The use of redox-active chemical probes can provide insight into sites that have been proposed experimentally and computationally.

Chalcogenide ions have been proposed as redox-active sites on the QD surface, though specific defect subpopulations can be quite challenging to probe experimentally.[7,24,29,53] In particular, oxidized S^{1-} species are expected to exist as stable disulfide dimers on as-synthesized QD surfaces.[24] To probe the presence of surface disulfides, studies were performed using a selective redox-active chemical probe. Tri-*n*-butylphosphine (Bu_3P) has been established to selectively reduce organic diselenides and disulfides.[24,54] Experiments in our lab confirm this reactivity for diphenyl disulfide, which is readily reduced to sulfates upon addition of Bu_3P in the presence of NaOH, yielding tri-*n*-butylphosphine oxide as a byproduct that may be monitored by $^{31}P\{^1H\}$ NMR spectroscopy (**Figure S30**).

Scheme 2. Reduction of Disulfide Moieties Using Tri-*n*-butylphosphine

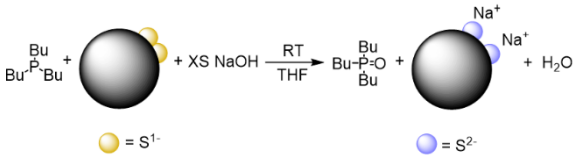

While reactions of Bu_3P with organic disulfides support the theory that disulfide dimers on QD surfaces may be reducible, to the best of our knowledge the presence of these chalcogenide dimers on individual QD surfaces has not yet been directly experimentally confirmed. To study this directly, PbS QDs were treated with Bu_3P in the presence of NaOH and monitored by $^{31}P\{^1H\}$ NMR spectroscopy for evidence of Bu_3PO formation as a handle for disulfide reduction (**Scheme 2**). Notably, as demonstrated by a lack of broad features in the $^{31}P\{^1H\}$ NMR spectra, Bu_3P does not appear to bind to the PbS QD surface (**Figure S31**). Addition of approximately 1000 equiv. Bu_3P to solutions of PbS QDs in THF in the presence of 50 equiv. NaOH led to differing results for small (3.4 - 3.7 nm) versus large (4.7 – 5.1 nm) QD samples. Smaller QDs show very little reactivity; little to no Bu_3PO formation was observed even over several days (**Figure S32**). By comparison, in larger QDs, approximately 1 of the added Bu_3P (ca. 10 equiv./QD) was converted to Bu_3PO, indicating reactivity of the phosphine with surface disulfides (**Figure 7**). This size dependence may arise from the influence of morphology and surface stoichiometry on the relative population of these disulfide traps, where larger QDs may reveal disulfides on exposed (100) facets that are not present on smaller, octahedral nanocrystals. These results suggest that the (100) facets and (100)/(111) facet edges may be the most likely sites for disulfide defects to arise. Importantly, under the conditions employed we did not detect any reaction between Bu_3P and $Pb(oleate)_2$, confirming that the observed reactivity was due to surface sulfide species (**Figure S33**).

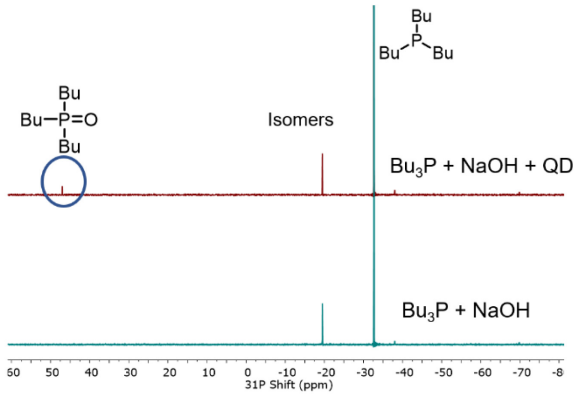

Figure 7. $^{31}P\{^1H\}$ NMR spectrum of (red) Bu_3P (28 mM) in THF with NaOH in degassed water. (blue) 5.1 nm PbS QDs (29 μM) in THF with ~1000 equiv. Bu_3P and 50 equiv. NaOH in degassed water.

Lewis bases such as trialkylphosphines are known to displace Z-type ligands from QD surfaces at high concentrations; as such, it was important to rule out $Pb(oleate)_2$ displacement as a primary cause for the disulfide reactivity detected.[21,22,30] Specifically, we sought to determine whether the reactivity observed was caused by Bu_3P first displacing $Pb(oleate)_2$ to reveal underlying disulfide structures. ^1H NMR spectra show minimal change in bound versus free ligand populations (**Figure S34 – S35**) of both 3.4 and 4.7 nm QDs with 1000 equiv. Bu_3P added, suggesting that this is not a dominant mechanism for the observed reactivity. Overall, the studies with a selective redox active probe, Bu_3P, provide compelling evidence for the existence and reactivity of surface disulfides. This work therefore serves as an example of using targeted experimental approaches to confirm or rule out the existence of hypothesized defect structures at QD surfaces.

4. Conclusions

In conclusion, through the use of a range of outer sphere reductants and selective redox reagents, we have gained an understanding of the native defects that exist on PbS QDs as well as those that are induced upon surface charging. Systematic investigations of the reactivity of the QD surfaces by NMR spectroscopy reveal oleate ligand displacement in response to reduction of surface Pb^{2+} ions. Comparison of the extent of ligand displacement across QD batches reveals a distinct size dependence, with larger QDs exhibiting a higher degree of ligand loss. This size-dependent surface reactivity correlates with known changes in PbS QD morphology with size.[22,30,31] Specifically, the emergence of new Pb^{2+} ion environments at (100) facets, and the edge sites between (100) and (111) facets, are proposed to be the primary Pb species reduced leading to oleate displacement. Furthermore, we demonstrate that the strength of the reductant employed has a significant impact on the extent of surface charging and reactivity; stronger reducing agents result in a greater amount of overall ligand displacement, whereas weak reducing agents show minimal reactivity with the QDs. Finally, the reactivity of chalcogenide-based defects (disulfides) was explored using a selective trialkylphosphine reagent. Similar to reduction of Pb ions, disulfide reactivity displays a distinct size dependence with more reactivity observed for disulfide reduction in larger QDs.

Taken together, these studies suggest that there is a larger relative proportion of redox-active defect

sites (both metal- and chalcogenide-based) present on larger PbS QDs. We argue that this size dependence is not simply because of increased surface area and total number of atoms in larger QDs; rather, changes in morphology correlated with increasing QD diameter leads to the formation of the redox-active defect sites probed herein. Overall, we present an example of using a powerful tool—chemical probes—in tandem with NMR spectroscopy to study the identity and reactivity of subpopulations of defect sites on QD surfaces.

Importantly, we view this work as a stepping stone for the field towards establishing a detailed, molecular-level picture of QD surfaces by employing multiple complementary techniques and targeted reactions.[19] We hope that future works will build upon these findings to further understanding of the structural nature of defect sites and their reactivity with added charge. The QD field is now, more than ever, poised to do so through the recent emergence of new tools to study QD surface structure, including advanced multinuclear NMR spectroscopy methods (e.g., probing metal or chalcogen nuclei directly, or using dynamic nuclear polarization or cross-polarization magic-angle spinning enhancement methods, etc.)[55–61] and innovative computational tools to explore surface structure motifs.[6,7,28,62] Such an approach is critical to gaining a molecular-level understanding of QD surfaces, and reaching the full potential of QD-based systems.

ASSOCIATED CONTENT

Supporting Information. Additional synthesis and characterization details, additional experimental data including TEM, NMR, XPS, and UV-Vis-NIR absorbance spectra. This material is available free of charge via the Internet at http://pubs.acs.org.

AUTHOR INFORMATION

Corresponding Author

* Jillian L. Dempsey
e-mail: dempseyj@email.unc.edu

Acknowledgments

This material is based upon work supported by the Air Force Office of Scientific Research under AFOSR Award No. FA9550-16-1-0206. CLH acknowledges support from the National Science Foundation Graduate Research Fellowship Program (DGE-1650116) and a UNC Chemistry Dobbins Award. J.L.D. acknowledges support from a Packard Fellowship in Science and Engineering. A portion of this work was performed using the UV-Vis-NIR absorption spectroscopy, Raman, and FTIR spectrometers in the CHASE Hub Instrumentation Facility established by the Center for Hybrid Approaches in Solar Energy to Liquid Fuels (CHASE), an Energy Innovation Hub funded by the U.S. Department of Energy, Office of Science, Office of Basic Energy Sciences under Award Number DE-SC0021173. This work made use of X-ray Photoelectron Spectroscopy instrumentation at the Chapel Hill Analytical and Nanofabrication Laboratory (CHANL), a member of the North Carolina Research Triangle Nanotechnology Network (RTNN), which is supported by the National Science Foundation (Grant ECCS-1542015) as part of the National Nanotechnology Coordinated Infrastructure (NNCI). A portion of this work was performed at the Analytical Instrumentation Facility (AIF) at North Carolina State University, which is supported by the State of North Carolina. This work made use of instrumentation at AIF acquired with support from the National Science Foundation (DMR-1726294). We thank the University of North Carolina' s Department of Chemistry NMR Core Laboratory for the use of their NMR spectrometers with support from the National Science Foundation under Grants No. CHE-0922858 and No. CHE-1828183. The authors thank Christian Y. Dones Lassalle for contributing a PbS QD sample to this project and Michael Mortelliti for assistance in TEM imaging. The authors thank Dr. Carrie Donley and Dr. Catherine McKenas for assistance in XPS measurements. C.L.H. thanks Melody Kessler, Michael Mortelliti, and Dr. Kedy Edme for helpful discussions.

References

(1) Kovalenko, M. V; Manna, L.; Cabot, A.; Hens, Z.; Talapin, D. V; Kagan, C. R.; Klimov, V. I.; Rogach, A. L.; Reiss, P.; Milliron, D. J.; et al. Prospects of Nanoscience with Nanocrystals. *ACS Nano* **2015**, *9*, 1012–1057.

(2) Carey, G. H.; Abdelhady, A. L.; Ning, Z.; Thon, S. M.; Bakr, O. M.; Sargent, E. H. Colloidal Quantum Dot Solar Cells. *Chem. Rev.* **2015**, *115*, 12732–12763.

(3) Kershaw, S. V.; Jing, L.; Huang, X.; Gao, M.; Rogach, A. L. Materials aspects of semiconductor nanocrystals for pptoelectronic applications. *Mater. Horiz.* **2017**, *4*, 155–205.

(4) Kodaimati, M. S.; McClelland, K. P.; He, C.; Lian, S.; Jiang, Y.; Zhang, Z.; Weiss, E. A. Viewpoint: Challenges in Colloidal Photocatalysis and Some Strategies for Addressing Them. *Inorg. Chem.* **2018**, *57*, 3659–3670.

(5) McClelland, K. P.; Weiss, E. A. Selective Photocatalytic Oxidation of Benzyl Alcohol to Benzaldehyde or C–C

Coupled Products by Visible-Light-Absorbing Quantum Dots. *ACS Appl. Energy Mater.* **2019**, *2*, 92–96.

(6) Giansante, C.; Infante, I. Surface Traps in Colloidal Quantum Dots: A Combined Experimental and Theoretical Perspective. *J. Phys. Chem. Lett.* **2017**, *8*, 5209–5215.

(7) Houtepen, A. J.; Hens, Z.; Owen, J. S.; Infante, I. On the Origin of Surface Traps in Colloidal II–VI Semiconductor Nanocrystals. *Chem. Mater.* **2017**, *29*, 752–761.

(8) Thomas, A.; Sandeep, K.; Somasundaran, S. M.; Thomas, K. G. How Trap States Affect Charge Carrier Dynamics of CdSe and InP Quantum Dots: Visualization through Complexation with Viologen. *ACS Energy Lett.* **2018**, *3*, 2368–2375.

(9) Brawand, N. P.; Goldey, M. B.; Vörös, M.; Galli, G. Defect States and Charge Transport in Quantum Dot Solids. *Chem. Mater.* **2017**, *29*, 1255–1262.

(10) Zou, H.; Dong, C.; Li, S.; Im, C.; Jin, M.; Yao, S.; Cui, T.; Tian, W.; Liu, Y.; Zhang, H. Effect of Surface Trap States on Photocatalytic Activity of Semiconductor Quantum Dots. *J. Phys. Chem. C* **2018**, *122*, 9312–9319.

(11) Kirkwood, N.; Monchen, J. O. V.; Crisp, R. W.; Grimaldi, G.; Bergstein, H. A. C.; du Fossé, I.; van der Stam, W.; Infante, I.; Houtepen, A. J. Finding and Fixing Traps in II–VI and III–V Colloidal Quantum Dots: The Importance of Z-Type Ligand Passivation. *J. Am. Chem. Soc.* **2018**, *140*, 15712–15723.

(12) van der Stam, W.; de Graaf, M.; Gudjonsdottir, S.; Geuchies, J. J.; Dijkema, J. J.; Kirkwood, N.; Evers, W. H.; Longo, A.; Houtepen, A. J. Tuning and Probing the Distribution of Cu^{+} and Cu^{2+} Trap States Responsible for Broad-Band Photoluminescence in $CuInS_2$ Nanocrystals. *ACS Nano* **2018**, *12*, 11244–11253.

(13) Veamatahau, A.; Jiang, B.; Seifert, T.; Makuta, S.; Latham, K.; Kanehara, M.; Teranishi, T.; Tachibana, Y. Origin of surface trap states in CdS quantum dots: relationship between size dependent photoluminescence and sulfur vacancy trap states. *Phys. Chem. Chem. Phys.* **2015**, *17*, 2850–2858.

(14) van der Stam, W.; du Fossé, I.; Grimaldi, G.; Monchen, J. O. V; Kirkwood, N.; Houtepen, A. J. Spectroelectrochemical Signatures of Surface Trap Passivation on CdTe Nanocrystals. *Chem. Mater.* **2018**, *30*, 8052–8061.

(15) Amelia, M.; Lincheneau, C.; Silvi, S.; Credi, A. Electrochemical properties of CdSe and CdTe quantum dots. *Chem. Soc. Rev.* **2012**, *41*, 5728 - 5743.

(16) Fedin, I.; Talapin, D. V. Probing the Surface of Colloidal Nanomaterials with Potentiometry *in Situ*. *J. Am. Chem. Soc.* **2014**, *136*, 11228–11231.

(17) Carroll, G. M.; Brozek, C. K.; Hartstein, K. H.; Tsui, E. Y.; Gamelin, D. R. Potentiometric Measurements of Semiconductor Nanocrystal Redox Potentials. *J. Am. Chem. Soc.* **2016**, *138*, 4310–4313.

(18) Chen, M.; Guyot-Sionnest, P. Reversible Electrochemistry of Mercury Chalcogenide Colloidal Quantum Dot Films. *ACS Nano* **2017**, *11*, 4165–4173.

(19) Hartley, C. L.; Kessler, M. L.; Dempsey, J. L. Molecular-Level Insight into Semiconductor Nanocrystal Surfaces. *J. Am. Chem. Soc.* **2021**, *143*, 1251–1266.

(20) Saniepay, M.; Mi, C.; Liu, Z.; Abel, E. P.; Beaulac, R. Insights into the Structural Complexity of Colloidal CdSe Nanocrystal Surfaces: Correlating the Efficiency of Nonradiative Excited-State Processes to Specific Defects. *J. Am. Chem. Soc.* **2018**, *140*, 1725–1736.

(21) Anderson, N. C.; Hendricks, M. P.; Choi, J. J.; Owen, J. S. Ligand Exchange and the Stoichiometry of Metal Chalcogenide Nanocrystals: Spectroscopic Observation of Facile Metal-Carboxylate Displacement and Binding. *J. Am. Chem. Soc.* **2013**, *135*, 18536–18548.

(22) Kessler, M. L.; Dempsey, J. L. Mapping the Topology of PbS Nanocrystals through Displacement Isotherms of Surface-Bound Metal Oleate Complexes. *Chem. Mater.* **2020**, *32*, 2561–2571.

(23) Hartley, C. L.; Dempsey, J. L. Electron-Promoted X-Type Ligand Displacement at CdSe Quantum Dot Surfaces. *Nano Lett.* **2019**, *19*, 1151–1157.

(24) Tsui, E. Y.; Hartstein, K. H.; Gamelin, D. R. Selenium Redox Reactivity on Colloidal CdSe Quantum Dot Surfaces. *J. Am. Chem. Soc.* **2016**, *138*, 11105–11108.

(25) Drijvers, E.; De Roo, J.; Martins, J. C.; Infante, I.; Hens, Z. Ligand Displacement Exposes Binding Site Heterogeneity on CdSe Nanocrystal Surfaces. *Chem. Mater.* **2018**, *30*, 1178–1186.

(26) Knowles, K. E.; Malicki, M.; Parameswaran, R.; Cass, L. C.; Weiss, E. A. Spontaneous Multielectron Transfer from the Surfaces of PbS Quantum Dots to Tetracyanoquinodimethane. *J. Am. Chem. Soc.* **2013**, *135*, 7264–7271.

(27) Pu, C.; Dai, X.; Shu, Y.; Zhu, M.; Deng, Y.; Jin, Y.; Peng, X. Electrochemically-stable ligands bridge the photoluminescence-electroluminescence gap of quantum dots. *Nat. Commun.* **2020**, *11*, 937.

(28) du Fossé, I.; ten Brinck, S.; Infante, I.; Houtepen, A. J. Role of Surface Reduction in the Formation of Traps in *n*-Doped II–VI Semiconductor Nanocrystals: How to Charge without Reducing the Surface. *Chem. Mater.* **2019**, *31*, 4575–4583.

(29) Voznyy, O.; Thon, S. M.; Ip, A. H.; Sargent, E. H. Dynamic Trap Formation and Elimination in Colloidal Quantum Dots. *J. Phys. Chem. Lett.* **2013**, *4*, 987–992.

(30) Choi, H.; Ko, J.-H.; Kim, Y.-H.; Jeong, S. Steric-

Hindrance-Driven Shape Transition in PbS Quantum Dots: Understanding Size-Dependent Stability. *J. Am. Chem. Soc.* **2013**, *135*, 5278–5281.

(31) Beygi, H.; Sajjadi, S. A.; Babakhani, A.; Young, J. F.; van Veggel, F. C. J. M. Surface chemistry of as-synthesized and air-oxidized PbS quantum dots. *Appl. Surf. Sci.* **2018**, *457*, 1–10.

(32) Moreels, I.; Lambert, K.; Smeets, D.; De Muynck, D.; Nollet, T.; Martins, J. C.; Vanhaecke, F.; Vantomme, A.; Delerue, C.; Allan, G.; et al. Size-Dependent Optical Properties of Colloidal PbS Quantum Dots. *ACS Nano* **2009**, *3*, 3023–3030.

(33) Jasieniak, J.; Califano, M.; Watkins, S. E. Size-Dependent Valence and Conduction Band-Edge Energies of Semiconductor Nanocrystals. *ACS Nano* **2011**, *5*, 5888–5902.

(34) Connelly, N. G.; Geiger, W. E. Chemical Redox Agents for Organometallic Chemistry. *Chem. Rev.* **1996**, *96*, 877–910.

(35) Koh, Wk.; Koposov, A. Y.; Stewart, J. T.; Pal, B. N.; Robel, I.; Pietryga, J. M.; Klimov, V. I. Heavily doped *n*-type PbSe and PbS nanocrystals using ground-state charge transfer from cobaltocene. *Sci. Rep.* **2013**, *3*, 2004.

(36) Shim, M.; Guyot-Sionnest, P. n-type colloidal semiconductor nanocrystals. *Nature* **2000**, *407*, 981–983.

(37) Hens, Z.; Martins, J. C. A Solution NMR Toolbox for Characterizing the Surface Chemistry of Colloidal Nanocrystals. *Chem. Mater.* **2013**, *25*, 1211–1221.

(38) Kessler, M. L.; Starr, H. E.; Knauf, R. R.; Rountree, K. J.; Dempsey, J. L. Exchange equilibria of carboxylate-terminated ligands at PbS nanocrystal surfaces. *Phys. Chem. Chem. Phys.* **2018**, *20*, 23649–23655.

(39) Knauf, R. R.; Lennox, J. C.; Dempsey, J. L. Quantifying Ligand Exchange Reactions at CdSe Nanocrystal Surfaces. *Chem. Mater.* **2016**, *28*, 4762–4770.

(40) Zhao, J.; Holmes, M. A.; Osterloh, F. E. Quantum Confinement Controls Photocatalysis: A Free Energy Analysis for Photocatalytic Proton Reduction at CdSe Nanocrystals. *ACS Nano* **2013**, *7*, 4316–4325.

(41) Rajh, T.; Micic, O. I.; Lawless, D.; Serpone, N. Semiconductor Photophysics. 7. Photoluminescence and Picosecond Charge Carrier Dynamics in Cadmium Sulfide Quantum Dots Confined in a Silicate Glass. *J. Phys. Chem.* **1992**, *96*, 4633–4641.

(42) Shiragami, T.; Fukami, S.; Wada, Y.; Yanagida, S. Semiconductor Photocatalysis: Effect of Light Intensity on Nanoscale Cadmium Sulfide-Catalyzed Photolysis of Organic Substrates. *J. Phys. Chem.* **1993**, *97*, 12882–12887.

(43) Nedoluzhko, A. I.; Shumilin, I. A.; Nikandrov, V. V. Coupled Action of Cadmium Metal and Hydrogenase in Formate Photodecomposition Sensitized by CdS. *J. Phys. Chem.* **1996**, *100*, 17544–17550.

(44) Pagels, N.; Prosenc, M. H.; Heck, J. An *ansa*-Cobaltocene with a Naphthalene Handle: Synthesis and Spectroscopic and Structural Characterization. *Organometallics* **2011**, *30*, 1968–1974.

(45) Zherebetskyy, D.; Scheele, M.; Zhang, Y.; Bronstein, N.; Thompson, C.; Britt, D.; Salmeron, M.; Alivisatos, P.; Wang, L. Hydroxylation of the surface of PbS nanocrystals passivated with oleic acid. *Science* **2014**, *344*, 1380–1384.

(46) Hendricks, M. P.; Campos, M. P.; Cleveland, G. T.; Jen-La Plante, I.; Owen, J. S. A tunable library of substituted thiourea precursors to metal sulfide nanocrystals. *Science* **2015**, *348*, 1226–1230.

(47) Hines, M. A.; Scholes, G. D. Colloidal PbS Nanocrystals with Size-Tunable Near-Infrared Emission: Observation of Post-Synthesis Self-Narrowing of the Particle Size Distribution. *Adv. Mater.* **2003**, *15*, 1844–1849.

(48) Houtepen, A. J.; Vanmaekelbergh, D. Orbital Occupation in Electron-Charged CdSe Quantum-Dot Solids. *J. Phys. Chem. B* **2005**, *109*, 19634–19642.

(49) Elgrishi, N.; Kurtz, D. A.; Dempsey, J. L. Reaction Parameters Influencing Cobalt Hydride Formation Kinetics: Implications for Benchmarking H_2-Evolution Catalysts. *J. Am. Chem. Soc.* **2017**, *139*, 239–244.

(50) Brozek, C. K.; Hartstein, K. H.; Gamelin, D. R. Potentiometric Titrations for Measuring the Capacitance of Colloidal Photodoped ZnO Nanocrystals. *J. Am. Chem. Soc.* **2016**, *138*, 10605–10610.

(51) Brown, P. R.; Kim, D.; Lunt, R. R.; Zhao, N.; Bawendi, M. G.; Grossman, J. C.; Bulović, V. Energy Level Modification in Lead Sulfide Quantum Dot Thin Films through Ligand Exchange. *ACS Nano* **2014**, *8*, 5863–5872.

(52) Harris, R. D.; Bettis Homan, S.; Kodaimati, M.; He, C.; Nepomnyashchii, A. B.; Swenson, N. K.; Lian, S.; Calzada, R.; Weiss, E. A. Electronic Processes within Quantum Dot-Molecule Complexes. *Chem. Rev.* **2016**, *116*, 12865–12919.

(53) Tsui, E. Y.; Carroll, G. M.; Miller, B.; Marchioro, A.; Gamelin, D. R. Extremely Slow Spontaneous Electron Trapping in Photodoped *n*-Type CdSe Nanocrystals. *Chem. Mater.* **2017**, *29*, 3754–3762.

(54) Humphrey, R. E.; Potter, J. L. Reduction of Disulfides with Tributylphosphine. *Anal. Chem.* **1965**, *37*, 164–165.

(55) Aebli, M.; Piveteau, L.; Nazarenko, O.; Benin, B. M.; Krieg, F.; Verel, R.; Kovalenko, M. V. Lead-Halide Scalar Couplings in ^{207}Pb NMR of $APbX_3$ Perovskites (A = Cs, Methylammonium, Formamidinium; X = Cl,

Br, I). *Sci. Rep.* **2020**, *10*, 8229.

(56) Piveteau, L.; Morad, V.; Kovalenko, M. V. Solid-State NMR and NQR Spectroscopy of Lead-Halide Perovskite Materials. *J. Am. Chem. Soc.* **2020**, *142*, 19413–19437.

(57) Chen, Y.; Smock, S. R.; Flintgruber, A. H.; Perras, F. A.; Brutchey, R. L.; Rossini, A. J. Surface Termination of $CsPbBr_3$ Perovskite Quantum Dots Determined by Solid-State NMR Spectroscopy. *J. Am. Chem. Soc.* **2020**, *142*, 6117–6127.

(58) Piveteau, L.; Ong, T.-C.; Walder, B. J.; Dirin, D. N.; Moscheni, D.; Schneider, B.; Bär, J.; Protesescu, L.; Masciocchi, N.; Guagliardi, A.; et al. Resolving the Core and the Surface of CdSe Quantum Dots and Nanoplatelets Using Dynamic Nuclear Polarization Enhanced PASS–PIETA NMR Spectroscopy. *ACS Cent. Sci.* **2018**, *4*, 1113–1125.

(59) Lee, D.; Wolska-Pietkiewicz, M.; Badoni, S.; Grala, A.; Lewiński, J.; De Paëpe, G. Disclosing Interfaces of ZnO Nanocrystals Using Dynamic Nuclear Polarization: Sol-Gel versus Organometallic Approach. *Angew. Chemie Int. Ed.* **2019**, *58*, 17163–17168.

(60) Zhang, J.; Zhang, H.; Cao, W.; Pang, Z.; Li, J.; Shu, Y.; Zhu, C.; Kong, X.; Wang, L.; Peng, X. Identification of Facet-Dependent Coordination Structures of Carboxylate Ligands on CdSe Nanocrystals. *J. Am. Chem. Soc.* **2019**, *141*, 15675–15683.

(61) Hanrahan, M. P.; Stein, J. L.; Park, N.; Cossairt, B. M.; Rossini, A. J. Elucidating the Location of Cd^{2+} in Post-synthetically Treated InP Quantum Dots Using Dynamic Nuclear Polarization ^{31}P and ^{113}Cd Solid-State NMR Spectroscopy. *J. Phys. Chem. C* **2021**, *125*, 2956–2965.

(62) Singh, S.; Tomar, R.; ten Brinck, S.; De Roo, J.; Geiregat, P.; Martins, J. C.; Infante, I.; Hens, Z. Colloidal CdSe Nanoplatelets, A Model for Surface Chemistry/Optoelectronic Property Relations in Semiconductor Nanocrystals. *J. Am. Chem. Soc.* **2018**, *140*, 13292–13300.

Table of Contents Graphic: